Proceedings World Geothermal Congress 2015
Melbourne, Australia, 19-25 April 2015

Geothermal, Structural and Petrophysical Characteristics of Buntsandstein Sandstone Reservoir (Upper Rhine Graben, France)

Sébastien Haffen[1], Yves Géraud[1] and Marc Diraison[2]

[1]Université de Lorraine – ENSG, 2 rue du Doyen Marcel Roubault, 54518 Vandœuvre-lès-Nancy, France

[2]Institut de Physique du Globe (IPG), UMR 7516 CNRS-Université de Strasbourg/EOST, 1 rue Blessig, 67084 Strasbourg Cedex, France

sebastien.haffen@univ-lorraine.fr yves.geraud@univ-lorraine.fr marc.diraison@iufm.unistra.fr

Keywords: petrophysics, structural geology, sandstone reservoir, fluid circulation

ABSTRACT

Buntsandstein (lower Triassic) sandstone reservoir located in the Upper Rhine Graben (Western Europe) appears as an easy target for geothermal exploitation. This reservoir links thick sandstone formation, more or less argillaceous, with a regional thermal anomaly.

Petrophysical measurements, including porosity by mercury injection, permeability (air and nitrogen), thermal conductivity and P-waves velocity, were performed on air and water saturated cores of EPS1 borehole (Soultz-sous-Forêts, France) in order to characterise Buntsandstein sandstone reservoir properties. Temperature gradient analysis, made from (1) thermal conductivity measurements performed on cores and (2) a temperature profile, suggest that fluid flow occurs locally in the reservoir. Petrophysical measurements and structural analysis of flow zones suggest that they are controlled first by a macroscopic network: with two major fault zones, and second by a matrix network: formed by sedimentary or diagenetic processes within two distinguishable facies: the Playa-lake and Fluvio-aeolian marginal erg facies.

In order to validate the previous proposed methodology and reservoir model, we propose to simulate fluid flow in the Buntsandstein reservoir applying TOUGH2 software and using the temperature profile from the static reservoir model. This model integrates the lithostratigraphy determined from cores observation, represented by horizontal layers, and two faults corresponding to the Soultz-sous-Forêts horst boundary, represented by vertical layers. Petrophysical characteristics are integrated using previous measurements. Two cases are tested. In the first case, the temperature profile is determined by a model with no fluid circulation between faults, heat transfer is governed only by conduction. In the second case, the temperature profile is determined by a model with fluid flow between faults. In the first case same overpressures (10 bars) are applied at the base of both faults, whereas in the second case two different pressures are applied (5 and 10 bars). The temperature profile obtained in the first case shows a global trend opposite to that measured in the borehole. In contrast, the temperature profile obtained in the second case indicates a global trend similar to that measured in the borehole. In the last case, fluid circulation occurs within faults zones and three lithostratigraphic levels, previously identified as fluid circulation zones in the reservoir. The differential pressure between faults driving the fluid flow inside the rock units could be explained by a tilt of the horst as observed at Soultz-sous-Forêts.

Data obtained from the thermal gradient analysis are compared to those obtained from different outcrops analyses. Two 3D conceptual models were built for the Buntsandstein sandstones reservoir of the Upper Rhine Graben: the first model integrated solely fractures of the reservoir, while the second one integrated fractures, sedimentology and fluid flow data. These models are provide new kind of data important for future reservoir exploration and exploitation.

1. INTRODUCTION

The Upper Rhine Graben, limited by a regional thermal anomaly associated with local anomalies along its borders (Munck, 1979; Pribnow and Schellschmidt, 2000), is a target for geothermal exploitation. In this regional context, several geothermal projects have started with the aim to exploit warm Rhine Graben reservoirs. In particular, Soultz-sous-Forêts Enhanced Geothermal System utilizes an artificial heat exchanger targeting the deep Hercynian crystalline basement, whereas other projects target the sandstone or sandstone/granite interface (Rittershoffen in France, Landau in Germany). This sandstone formation, overlying the basement, corresponds to the Buntsandstein sandstone reservoir that previously studied to evaluate its geothermal potential (Dezayes et al., 2007). Provided this sandstone formation is a good aquifer and is connected to the granite reservoir, it could be directly exploited to produce geothermal energy at low drilling costs.

The geothermal gradient measured at Soultz-sous-Forêts (Pribnow et al., 1999) is about 105°C/km in the Upper Triassic levels, it progressively decreases through the Buntsandstein sandstone and in the upper granitic basement, and increases again at about 3000 m depth. This could be explained by both the contrast of thermal conductivities between the sedimentary cover and the granite and the presence of natural conductive heat transfer levels at the top of the granite (Le Carlier et al., 1994). Moreover, previous works showed that the thermal anomaly in the Rhine graben can be related to vertical circulation of thermal water along faults (Bächler, 2003; Kohl, 2000).

In order to characterize the fluid flow pattern and the heat diffusion and convection processes in the sandstone formation, petrophysical properties were measured on cores from borehole EPS1 in Soultz-sous-Forêts (Haffen, 2012). A first evaluation of the fluid flow pattern within the Buntsandstein sandstone formation was performed (Haffen et al., 2013) and theoretical and measured geothermal gradient logs were compared. The theoretical gradient was calculated using thermal conductivities data and the Fourier law, while the measured one was derived from the temperature logged in the borehole EPS1. In a second evaluation, we

intended to determine which flow conditions applied to the crossing faults could explain the observed anomalies in the geothermal gradient at Soultz-sous-Forêts, and therefore, demonstrate numerically that only inter-fault flows through these layers could explain the temperature gradient anomalies. A two-dimensional (2D) vertical conceptual model was defined that integrates the different horizontal lithostratigraphic layers associated with petrophysical properties measured on cores, and that is bounded laterally with two vertical faults. Several flow and heat transport simulations were carried out using TOUGH2 (Pruess et al., 1999) based on different pre-defined flow and temperature boundary conditions.

Data obtained from the thermal gradients analysis are associated to those obtained from different outcrops analyses. A 3D conceptual model has been built for the Buntsandstein sandstones reservoir of the Upper Rhine Graben, integrating reservoir fractures, sedimentological characteristics and fluid flow zones. This model provides new kind of data important for future reservoir exploration and exploitation.

2. GEOLOGICAL SETTING AND BOREHOLE DESCRIPTION

The Soultz-sous-Forêts borehole EPS1 is located in the French part of the Upper Rhine Graben, near its western boundary marked by the Rhine Fault (Figure 1). The graben, which is 30-40 km wide and extends NNE-SSW over a distance of 300 km, forms part of the western European Cenozoic Rift System. Fault traces maps, proposed by Valley (2007), provide an idea of the orientation of major structures affecting the graben: (1) a N0°-N20°E trend, called Rhenish direction, corresponds to normal faulting forming the Upper Rhine Graben, and was originated during the its Oligocene opening (Schumacher, 2002), (2) the Erzgebirgian NE to ENE trend (Edel and Weber, 1995) corresponding to the general Hercynian orientation with major Variscan dislocation zones dominating this direction, and (3) NW-SE structures, relatively rare in the Cenozoic sediments filling, but mainly present in the border of the graben in pre-Cenozoic rocks. At local scale, in the Soultz-sous-Forêts area, same dominant orientations are present along with others: NNW-SSE and WNW-ESE striking structures (Genter, 1990).

Borehole EPS1, drilled through the sedimentary cover and into the basement, was cored continuously from a depth of 930 m, in the Muschelkalk limestone, to a depth of 2220 m in the Palaeozoic granite (Vernoux et al., 1995) (Figures 1 & 2). The cores provide a continuous vertical section through the geothermal Buntsandstein reservoir; located between depths of 1008.90 m and 1416.77 m.

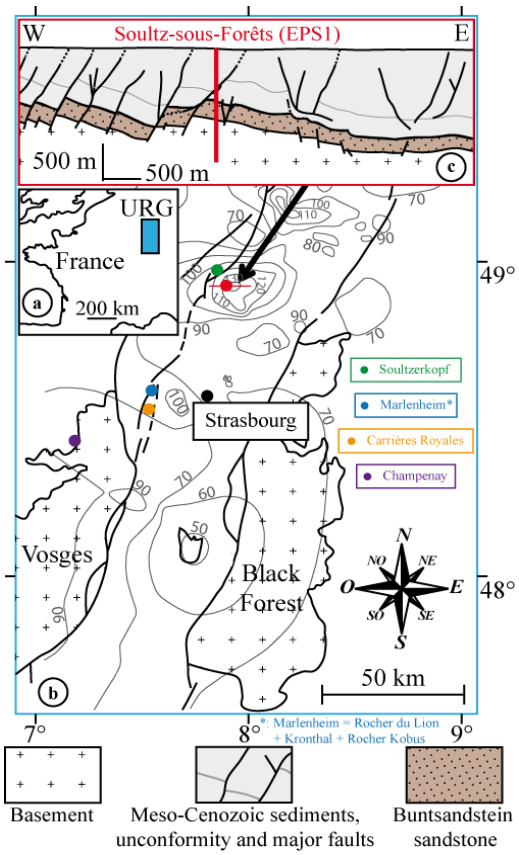

Figure 1: a) Location of the Upper Rhine Graben (URG) in Western Europe. b) Upper Rhine Graben map; red dot and line (Soultz-sous-Forêts) denote the location of borehole EPS1 and the geological cross-section (c) respectively; the grey lines indicate the temperature at 1500 m depth based on data from GGA Hannover (Genter et al., 2004; Pribnow and Schellschmidt, 2000). Green, blue, yellow and violet dots locate outcrops analyzed for this study. c) Soultz-sous-Forêts geological cross-section (redrawn after Place et al., 2010) showing the approximate location of borehole EPS1 at depth.

Sizun (1995) and Vernoux et al. (1995) have provided descriptions of the sedimentary cores (Figure 2a). The basal Permian Sandstone (1416.77-1407.70 m) and Annweiler Sandstone (1407.70-1349.15 m) are interpreted as distal braided fluvial networks in which sandy channels alternate with finer flood-plain and lacustrine deposits. The overlying Vosgian Sandstone (1349.15-1084.80

m) comprises two units: the Lower Vosgian Sandstone from the bottom of the unit to 1176.00 m, and the Upper Vosgian Sandstone from 1176.00 m to the top of the unit. Bourquin et al. (2009) proposed a detailed stratigraphic column with genetic units based on a sedimentary and gamma-ray analysis of the Vosgian Sandstone. They suggest that the Lower and Upper Vosgian Sandstone are made up of three sedimentary facies distinguished by their mode of deposition: braided river deposits within an arid alluvial plain (1349-1243 m; 1215-1183 m; 1112-1084 m), Playa-Lake deposits and fluvial and aeolian sand sheets (1183-1112 m), and fluvial-aeolian marginal erg deposits (1243-1215 m). The Intermediate Beds, located between 1084.80 and 1020.50 m, can be subdivided into four units: (1) the Obere Felsone (1084.80-1064.50 m), (2) the Bitche Conglomerate (1064.50-1060.00 m), (3) the Middle Intermediate Beds (1060.00-1044.00 m) and (4) the Upper Intermediate Beds (1044.00-1020.50 m). Intermediate Beds reflect a braided fluvial system characterised by thinner and more differentiated sequences than the thick generally homogenous Vosgian Sandstone sequences. The Voltzia Sandstone, the uppermost formation of the Buntsandstein succession (1020.50-1008.90 m) reflects a transition to the lagoonal argillaceous deposits of the Muschelkalk.

Natural fracturing was analysed in the continuous oriented cores using borehole images (Genter et al., 1997) (Figure 2c, d). The fracture trends were determined by the tectonic history of the Upper Rhine Graben area with a probable reactivation of some Hercynian structures. A total of 325 fractures have been identified along the 408 m of core, with seven different fracture-density zones (Figure 2c, d). The mean fracture density of the sedimentary sequence is 0.81 fractures/m. The highly fractured zones (1) and (4) are both associated with the presence of a major fault (Vernoux et al., 1995) known as the Soultz Fault in the upper part of the borehole. The distribution of fracture apertures measured in cores shows a close relationship with the fractures at depth (Vernoux et al., 1995), with the largest apertures located within the high-density fracture zones.

A temperature log (Figure 2b), undisturbed by drilling operations such as mud circulation, was run in borehole EPS1 in November 1991, nine months after the completion of drilling and when the well was in thermal equilibrium. The log provides temperature values at one meter intervals through the sandstone, with temperatures ranging from 120.24 °C at the top of the Buntsandstein (1009.19 m) to 136.45 °C at the bottom (1415.95 m). The mean geothermal gradient in this part of the borehole is 39.85 °C/km.

3. FLUID FLOW LOCALIZATION FROM TEMPERATURE GRADIENTS ANALYSIS

3.1 Methodology

With the aim of localizing the fluid flow in the Buntsandstein reservoir intersected by borehole EPS1, we propose an approach based on thermal gradients analysis in a borehole once thermal equilibrium is reached (Haffen et al., 2013). The method compares two sets of thermal gradients (figure 2e). The first set corresponds to thermal gradients calculated using Fourier's law from the estimated heat-flow at the bottom of the formation and the thermal conductivity measured on rock samples. It results in an estimated conductive thermal gradient that takes into account lithological heterogeneities. The second set corresponds to the thermal gradients determined from temperature logged in the borehole. It represents the real gradient induced by heat conduction from a deep heat source and also includes convective disturbances due to the circulation of hot or cold fluids. By comparing the two thermal gradient datasets from the same wellbore the location of fluid flow zones can be determined.

Heat flow (q) is given by the product of the thermal conductivity (λ) and the temperature gradient (dT/dz) according to Fourier's law (1D case):

$$q = -\lambda*(dT/dz) \quad (1)$$

The heat flow in the basal unit of borehole EPS1 represents the heat flux entering the sedimentary series from the granitic basement and is assumed to be constant across the sandstone reservoir in a system considered to be conductive. Because of the low amount of decaying radioactive elements, the heat production rate in the Buntsandstein sandstones is about 1 $\mu W/m^3$ (Schellschmidt and Clauser, 1996). This contribution is ignored in the heat flow calculation. In the present case, the thermal gradient was calculated from the measured thermal gradients in the borehole intersecting the Permian unit (29.76±1.44 $°C.km^{-1}$), and the mean thermal conductivity (3.17±0.47 $W.m^{-1}.K^{-1}$) was calculated from λ measured on the cores and corrected for the *in-situ* temperature according to the law proposed by Vosteen and Schellschmidt (2003). The heat flow through the basal unit, estimated using the calculated thermal gradient and thermal conductivity values, is about 94 $W.m^{-2}$. The thermal gradient was calculated for each core depth along the Buntsandstein series from the measured thermal conductivity, corrected for *in-situ* temperature and the knowledge of the heat flow determined above.

The thermal gradient was also calculated between each measured interval of the temperature log data (vertical resolution: ±1m). It appears relatively constant and low at the bottom part of the sedimentary series (thermal gradient through the Permian Sandstone: 29.99 $°C.km^{-1}$), increasing upwards toward the top of the Buntsandstein sandstones reservoir (thermal gradient through the Voltzia Sandstone: 71.15 $°C.km^{-1}$). The maxima values of thermal gradient within the Lower Vosgian Sandstone (at ~1220 m) and Upper Vosgian Sandstone (at ~1120 m) are about 48 and 59 $°C.km^{-1}$ respectively.

Two cases are highlighted (1) both the measured and calculated thermal gradients have similar values in a defined interval, then the heat transfer in this interval is apparently only governed by conduction without any hot or cold fluid circulation (NFZ, Figure 2e), and (2) measured gradients are higher than the calculated ones, then the difference between this two values could be the result of hot fluid circulation in this part of the borehole (FZ, Figure 2e). On both sides of the FZc, the thermal gradient is not disturbed in regard to the conductive one. In this part of the profile, the hot flow input in the FZc zone does not disturb the heat-flow in the surrounding formations.

The combination of the macroscopic flow/non-flow zones deduced from the thermal gradient analysis against the matrix permeability and porosity measurements (Figure 2f, g), sedimentary facies, and fracture distribution along the core, allows us to determine what factors control the hot fluid circulation.

3.2 Non-flow zones (NFZ)

Three zones were identified in borehole EPS1: (1) the top of the Playa Lake level *(NFZa)*, (2) the bottom of the Playa Lake level *(NFZb)*, and (3) the bottom part of the formation *(NFZc)* from 1235 m depth to the granite/sandstone contact. The first two zones are relatively thick and have low permeability and porosity. The third zone *(NFZc)* incorporates the Permian Sandstone, the Annweiler Sandstone and the first unit of braided river facies in the Lower Vosgian Sandstone. The lower part of the third zone is characterized by high permeability and porosity values, whereas the Annweiler Sandstone, Permian Sandstone and upper part of the first unit of braided river facies have relatively low permeability and porosity. This could be due to the macroscopic sedimentary facies with crossbeds and thick clayey beds forming a complex network of impermeable layers that reduces the macroscopic permeability, even though the matrix permeability and porosity are high. The highly fractured zone in the Annweiler Sandstone consists mainly of sealed fractures with few fractures showing small apertures that are insufficient for a network connection to the area of hot fluid feeding.

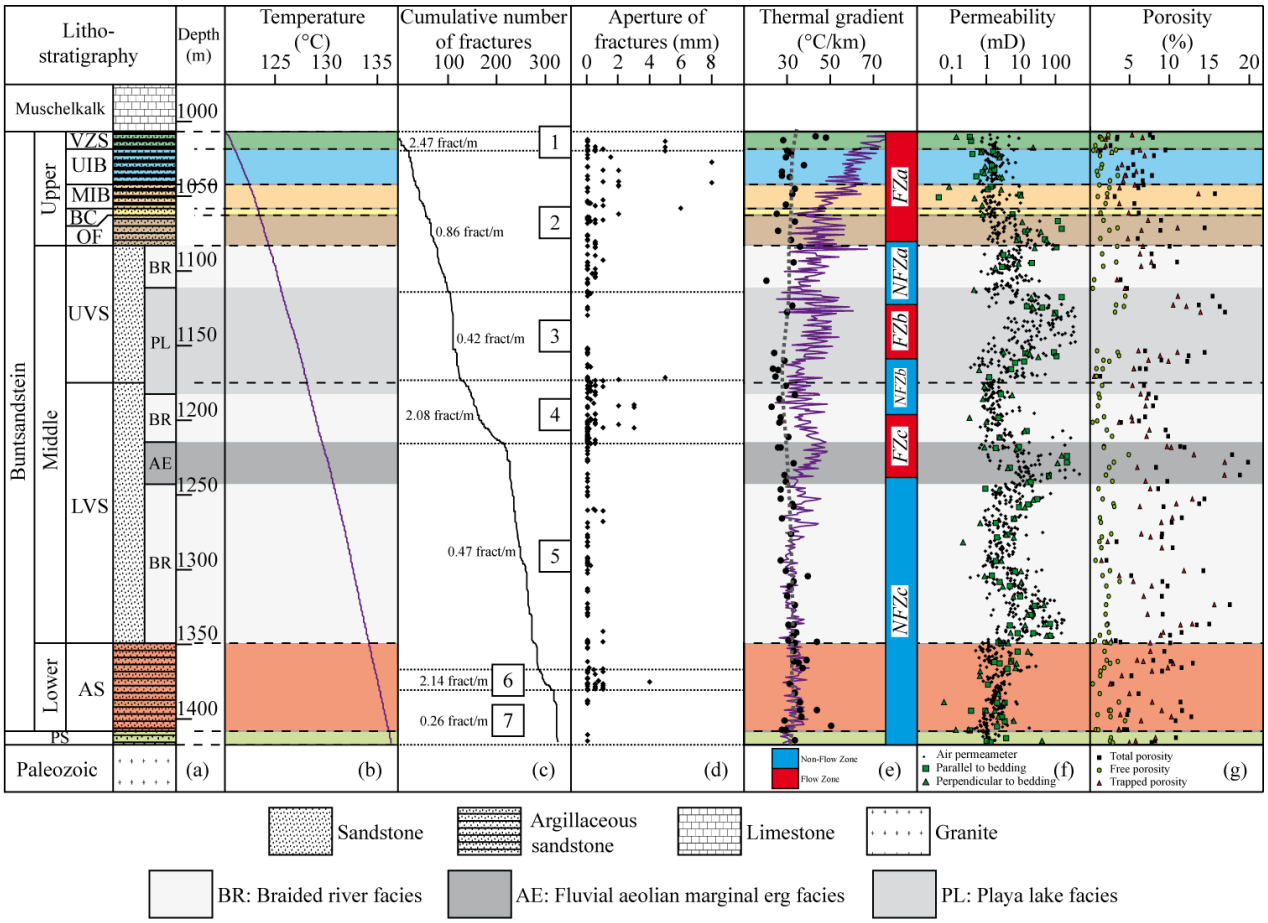

Figure 2: a) Synthetic stratigraphic column of the Buntsandstein in borehole EPS1 (modified after Sizun (1995) (VZS: Voltzia Sandstone; UIB: Upper Intermediate Beds; MIB: Middle Intermediate Beds; BC: Bitche Conglomerate; OF: Obere Felsone; UVS: Upper Vosgian Sandstone; LVS: Lower Vosgian Sandstone; AS: Annweiler Sandstone; PS: Permian Sandstone). b) Temperature log. c) Cumulative number of fractures. d) Apertures of fractures. e) Thermal gradient: violet line shows the thermal gradient determined from the temperature logs; solid black circles the thermal gradient calculated from thermal conductivity measurements on cores and from estimated conductive heat-flow, grey dotted line shows the averaged calculated thermal gradient. f) Permeability, black dots represent the air permeability measured with Tiny-perm II: grey squares correspond to permeability measured parallel to the stratification, and grey triangles correspond to permeability measured perpendicular to the stratification (Sizun, 1995). g) Porosity by mercury injection.

3.3 Flow zones (FZ)

Three main flow zones are recognized from top down to bottom: (1) the top of the Buntsandstein *(FZa)*, (2) the Playa Lake facies between 1130 and 1150 m *(FZb)*, and (3) the second Braided River facies and underlying Fluvio-Aeolian Marginal Erg facies between 1190 and 1235 m *(FZc)*. Although *FZa* is composed of low permeability and porosity sandstone, except in the Obere Felsone, the Buntsandstein in this part of the borehole contains fractured zones associated with the presence of a major fault. *FZb* is characterized by high matrix permeability and porosity values and very few sealed fractures, it is controlled mainly by sedimentary or diagenetic properties and it is connected with the deep hot fluid source through the westward-developed damage zone of the Soultz fault. For flow zone *FZc*, the bottom part in the fluvio-aeolian marginal erg facies has high matrix permeability and porosity, and few sealed fractures, whereas the top, in the braided river facies, has low matrix permeability and porosity, and high fracture density (fracture zone 4) with many large apertures forming the damage zone around a major fault zone. The open fractures in the

fault zone would appear to form a pathway for the deep hot fluids to flow into the underlying permeable Fluvio-Aeolian facies. Hot fluid circulation in fractured zones suggests that fractures remain open with depth in spite of lithostatic pressure.

3.4 Conceptual model

Analysis of the thermal gradients in borehole EPS1 has enabled us to locate permeable zones where hot fluid flows occur at formation scale in the Buntsandstein. Nevertheless, different pathways are needed to explain the observed thermal gradient anomalies. An upward-flowing path for hot fluids from the deep part of the basin is provided by fault zones. The damage zones associated with faults enable the upward flowing fluids to connect with the stratigraphic reservoirs ('horizontal layers'). Such transfer paths to the stratigraphic reservoirs are controlled mainly by sedimentary and diagenetic processes. The reservoirs in the Playa Lake and Fluvio-Aeolian Marginal Erg facies have high matrix permeability and an excellent horizontal connectivity. Conversely the Braided River facies, despite high matrix permeability, present a broad network of thick oblique argillaceous layers which decreases the macroscopic permeability.

The flow paths appear as a composite network controlled by both 'sedimentary' and 'fracture' permeability. Fracturing associated with the two fault zones provide pathways for the upward flowing fluids to connect with stratigraphic levels characterized by high matrix permeability layers. Thus, the Playa Lake and Fluvio-Aeolian Marginal Erg facies are a reservoir connected to a deep hot fluid source.

4. FRACTURE ANALYSIS AND BLOCK MODEL

Fracture pattern in Buntsandstein sandstones has been analysed both from EPS1 cores observations and from outcrops studies in the graben shoulders (figure 1). Selected outcrops (Haffen, 2012) allow fractures description in the different lithological facies of the reservoir and at different structural position.

Globally, Buntsandstein sandstones present low fracture density in central part of blocks, away from majors fault zones. However, fractures distribution evolved also according to their situation along the different sedimentary series.

Near Rhenish major fault zones, fractures appear organised in a corridor of high fracture density, separated by low density zones. This fracture organization was not recognized near Hercynian reactivated fault. Baryte and quartz precipitation have been observed near this last fault and near Rhenish oriented fault. However, none or rare mineral precipitation is observed in fractures localized in the central part of the block. These kinds of mineralization indicate paleo fluid flow. Furthermore, mineral precipitation is an important driver to fracture porosity and permeability decrease, and thus, constitute an important fluid flow gate.

All data, from borehole and outcrop studies, drive us to the building of a 3D conceptual model of the Buntsandstein reservoir located in the Upper Rhine Graben (Figure 3). This block model shows the regional sedimentary units and structures forming the reservoir. The used approach allows taking into account reservoir characteristics in the central part of a block and near major faults bounding them. The block is bounded by four faults representing the main tectonic accidents: two normal faults with N0°-N20°E trend and two Hercynian reactivated faults with N60°E and N130°E trend respectively. These two last faults are equivalent to the ones intersected by borehole EPS1 in the upper part of the reservoir. Buntsandstein sandstones are situated between Muschelkalk limestones and Palaeozoic granite. Permian sandstones are situated in a Permian basin. Blocks present a mean tilt toward the west of about 5°, equivalent to the tilt measured in the Soultz-sous-Forêts area. Note that the Buntsandstein reservoir model presents no scale. In fact, the distances between two faults range between kilometres and hectometres scale (Valley, 2007). Moreover, thicknesses of the Buntsandstein reservoir range between few meters in the South of the graben to more than 1600 m in its northern part (Dezayes et al., 2007). And finally, the depth of the contact sandstone/granite ranges between 450 and 4850 m, in function of the situation in the graben.

Buntsandstein lithological units are integrated into the model according to the description of the EPS1 borehole (Sizun, 1995; Vernoux et al., 1995). Note that each unit thickness is variable according to the position in the Upper Rhine Graben. Fluid circulation zones are integrated in the model according to thermal gradients analysis performed in borehole EPS1.

5. MODELING OF FLUID FLOW IN THE RESERVOIR

5.1 Conceptual model (fault block scale)

A simplified 2D form of this conceptual model was derived to conduct the phenomenological study using TOUGH2 flow and heat transport simulations for different boundary condition hypotheses. The objective being to identify flow paths through faults and permeable layers that can explain the temperature gradient anomalies, vertical faults and homogeneous horizontal layers were assumed (Figure 4). The model covers the Buntsandstein reservoir, from the Muschelkalk horizon at 980 m depth, and extends down to 14 m below the top of the granite reservoir at 1416 m depth (granite/sandstone interface depth). The layers correspond to the main lithostratigraphic units identified in borehole EPS-1 (Figure 2a). The natural fracture network is ignored. The model is bounded on the left and the right by two vertical conductive faults 1000 m apart. The fault thickness is assumed to be 1 m, according to Haffen (2012), who measured fault thicknesses ranging from 0.65 to 5m, and the permeability is 0.01 mD, according to Place et al. (2010). The model is 1000m wide, 10 m thick and 450m high. The corresponding TOUGH2 simulation grid is regular with 100×1×90 cells (Figure 4). For each layers, the associated petrophysical data are given in Haffen (2012).

5.2 THOUGH2 simulation scenarios

Different boundary condition scenarios were studied to identify the ones that are likely to explain the temperature gradient anomalies observed in EPS1. The thermal boundary conditions are the same for all scenarios. They are simply defined as prescribed temperatures at the top and the bottom, according to those measured in EPS1 (Figure 2b), with no heat flux laterally. The flow boundary conditions are scenario-dependent with defined pressures used at the top and bottom of each fault. No flow is assumed for all scenarios elsewhere. Depending on the pressures applied to the faults, vertical flow can be generated through the faults or horizontal flow through the permeable sedimentary layers. In this way, three types of scenarios were considered and Table 1 summarizes the pressure and temperature boundary conditions applied to each scenario.

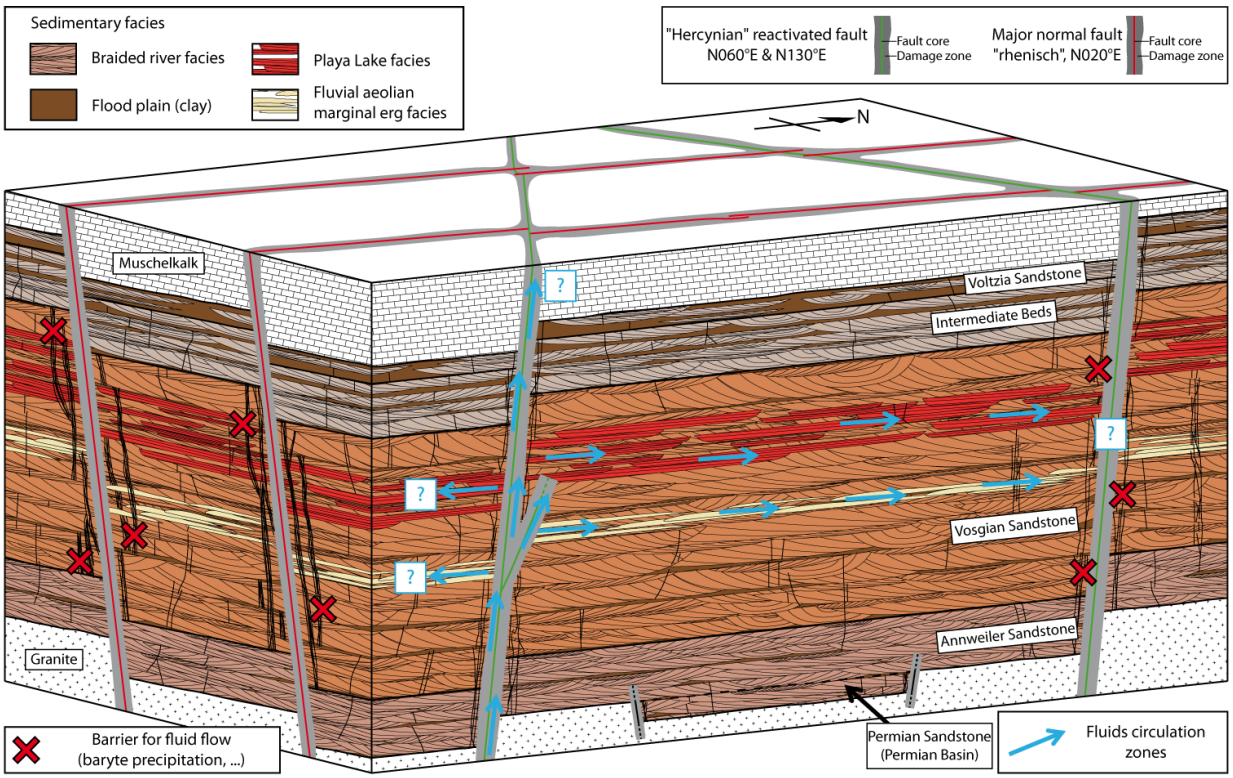

Figure 3: 3D conceptual model of a block, bounded by a set of major faults in the Buntsandstein sandstones formation located in the Upper Rhine Graben

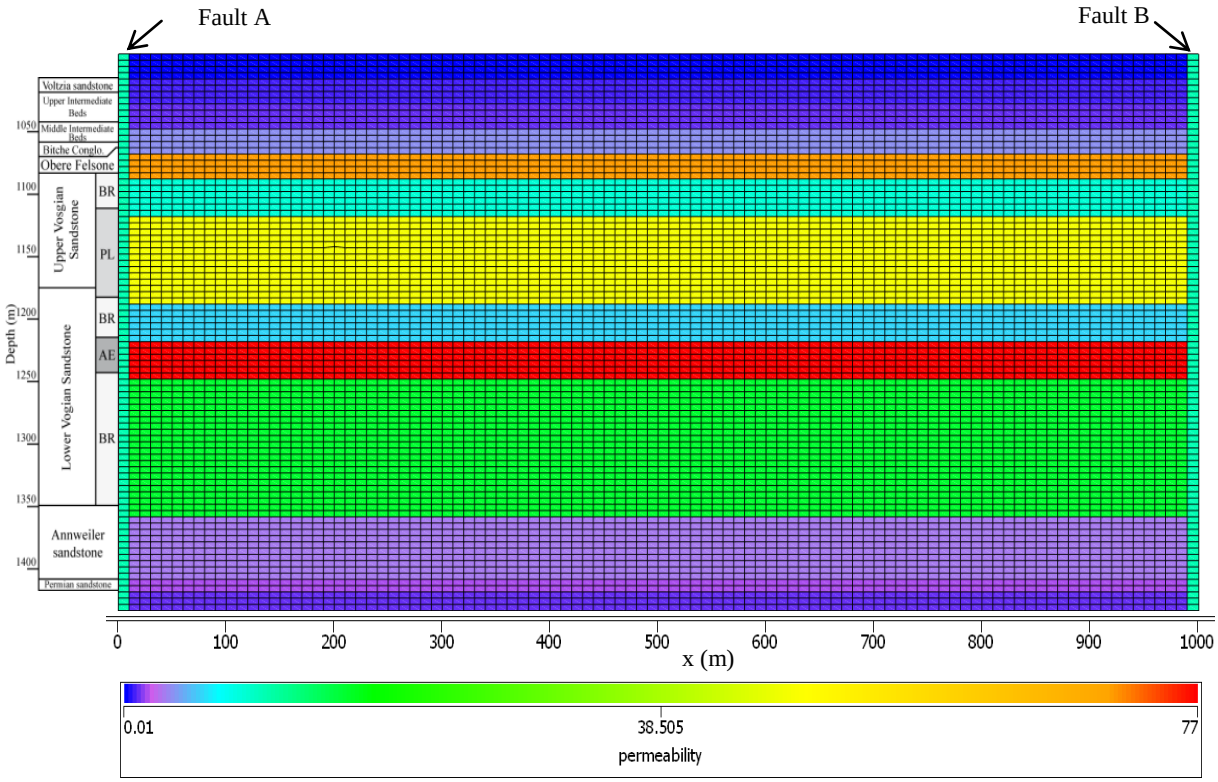

Figure 4: 2D numerical reservoir model (100×1×90 cells): layers and permeability (in mD)

Scenario 1: Hydrostatic conditions preventing fluids from flowing vertically from the granite reservoir through the faults. This scenario corresponds to purely diffusive heat transfer and is equivalent to the analytical gradient calculated with the Fourier law and measured thermal conductivities.

Table 1: Pressure and temperature boundary conditions applied to the top and the bottom of the model for each scenario

Scenario	Boundary condition	P (bar) Fault A	P (bar) Fault B	T (°C)
1	Top	96	96	117
	Bottom	136	136	137
2	Top	96	96	117
	Bottom	140	140	137
3	Top	96	101	117
	Bottom	140	145	137

Scenario 2: Same hydraulic potentials applied to the two faults allowing vertical flow through the faults but preventing fluids from flowing horizontally through the permeable sedimentary layers. This scenario corresponds to two conductive but no connected faults. Convective heat transport only takes place within the faults.

Scenario 3: Different hydraulic potentials applied to the two faults allowing both vertical flow through the faults and horizontal flow through the permeable sedimentary layers. This scenario corresponds to two conductive faults that are connected through the permeable sedimentary layers with convective heat transport taking place within both the faults and the permeable layers.

5.3 Comparison between measured and simulated temperature logs

The simulation of scenario 1 (purely diffusive heat transfer in hydrostatic conditions) is expected to show vertical temperature gradient logs similar to the analytical gradient calculated using the Fourier law (Figure 2e). This is true far enough from the faults, the distribution of thermal conductivities being different inside and outside the faults in the numerical model. Figure 5 shows the two analytical and numerical (simulated) temperature gradient logs. The analytical gradient looks more erratic with short scale variability, but both curves display the same trends. The differences can be explained by the smaller resolution of the numerical model, leading to averaged but less accurate gradients. A more appropriate gradient calculation method would have been to, first, smooth the calculated and simulated temperature logs, then to derive from them more reliable temperature gradients. Such an improvement was beyond the scope of this work. Nevertheless, this first comparison allowed us to validate the numerical heat diffusion model and to confirm that the numerical simulations provide consistent results that can be compared with measured geothermal gradients in order to study the effects of flow paths onto the temperature distribution.

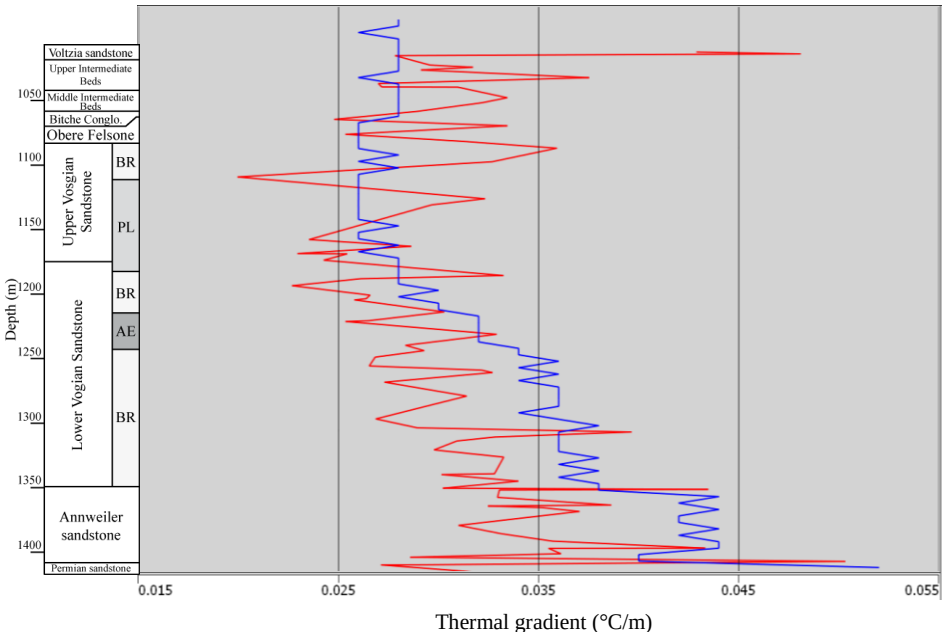

Figure 5: Comparison between the analytical temperature gradient calculated using Fourier's law and thermal conductivity measurements (in red), and the simulated temperature gradient for the hydrostatic conditions of scenario 1 (in blue)

The numerical temperature gradients obtained with scenarios 2 and 3 are depicted in Figure 6 together with the measured temperature gradient. The numerical gradients correspond to a distance of 40 m from fault A, which is the location where best fit of the measured temperature gradient was obtained as detailed later. Comparison of the measured and simulated temperature gradients shows that scenario 2 leads to an opposite global gradient trend (gradient increasing with depth), unlike scenario 3, which correctly reproduces the global trend and most local trend changes. These preliminary results tend to show that a convective heat transport only located in the faults cannot explain by itself the measured temperatures. The two faults must also be flow-connected through the permeable sedimentary layers to fit the trends.

The temperature distributions corresponding to scenarios 1 to 3 are illustrated in Figure 7. Whereas scenarios 1 and 2 lead to symmetrical temperature fields, scenario 3 reveals a more complex and nonsymmetrical temperature distribution, with higher

vertical spreading of temperatures leftwards, i.e., downstream with respect to flow through the permeable sedimentary layers. With scenario 1, the faults have very little impact on the temperature distribution. This is not true with scenarios 2 and 3, for which the vertical distribution of temperature depends on the distance to the faults, with the possible exception of scenario 2, beyond certain distance (about 100 m). More interesting, for scenario 3, it can be noticed that the vertical distribution of temperature can be used to determine whether the well is close to the downstream (left-hand) fault or the upstream (right-hand) one.

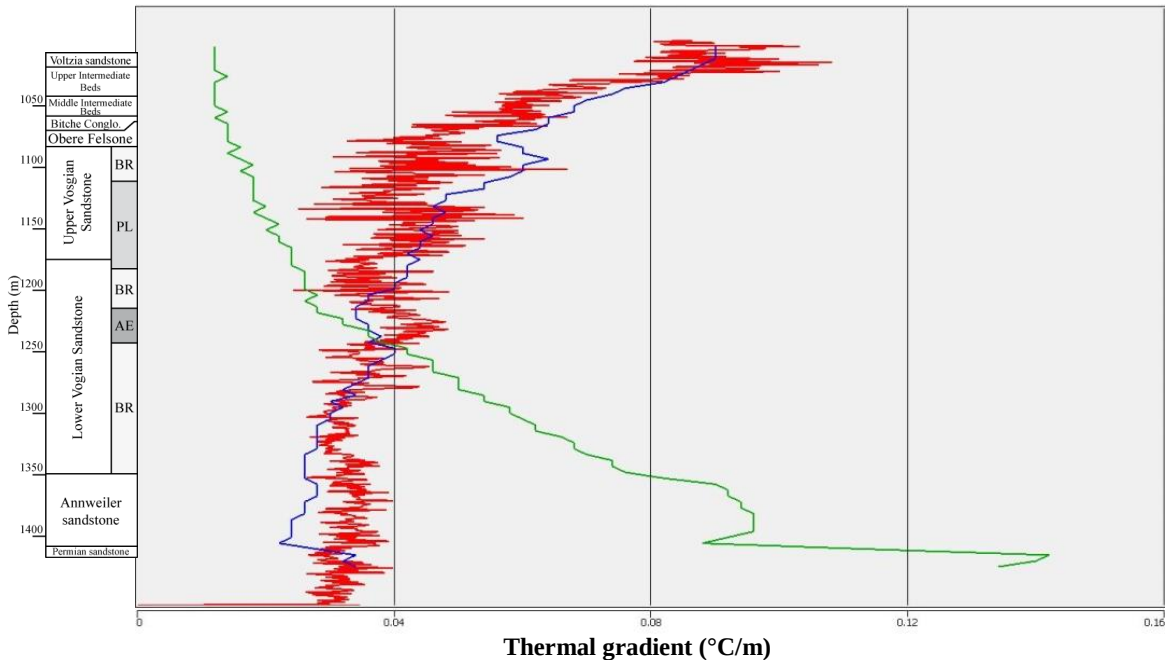

Figure 6: Comparison of the temperature gradient measured in borehole EPS1 (in red) with the simulated ones of scenario 2 (in green) and scenario 3 (in blue) at a distance of 40m from fault A

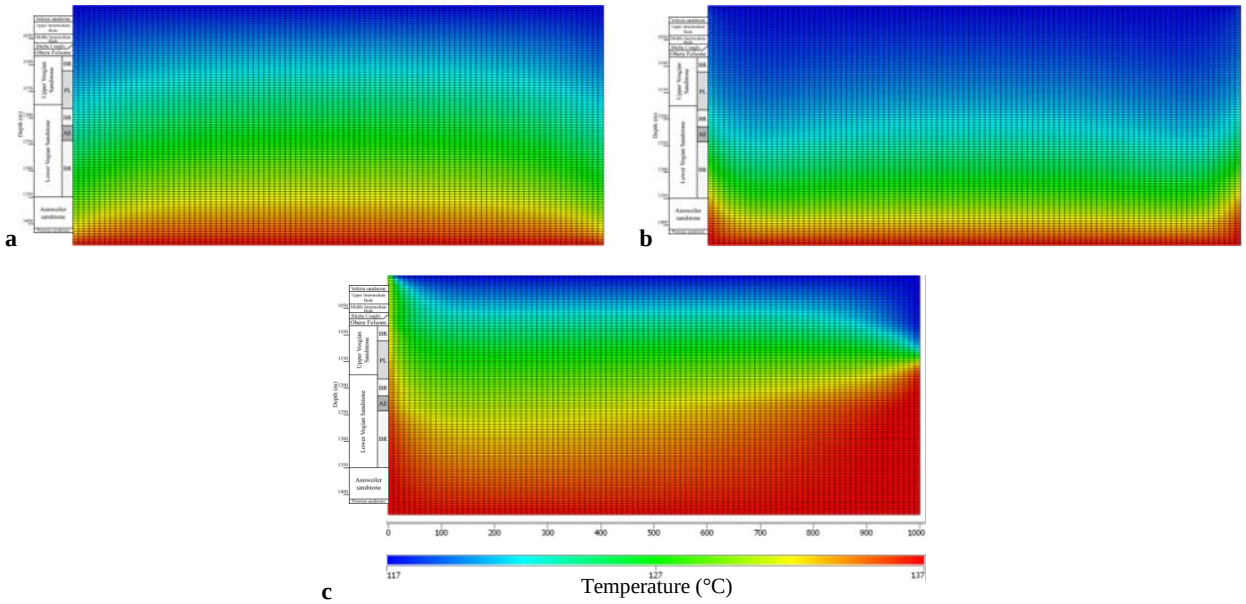

Figure 7: (a) Simulated steady-state temperature distributions for scenario 1 (purely diffusive heat transfer), (b) simulated steady-state temperature distributions for scenario 2 (convective heat transport in faults), (c) simulated steady-state temperature distributions for scenario 3 (convective heat transport in both faults and permeable layers)

The only available measured temperature log is from borehole EPS1, which is known to be not too far from a fault and can therefore be used to understand the flow pattern and the flow direction at the fault block scale. To do so, the temperature data from EPS1 are compared with the simulated temperature logs at various distances from the faults (Figure 8). At all distances, the simulated temperature curves of scenario 2 are "concave" and do not fit the global trend of measured temperatures. On the contrary, the vertical temperature distributions predicted by scenario 3 depict the expected (convex) shape and correctly fit the measured temperature log, as well as the temperature gradient log (Figure 6) at a distance of 40 m from (downstream) fault A.

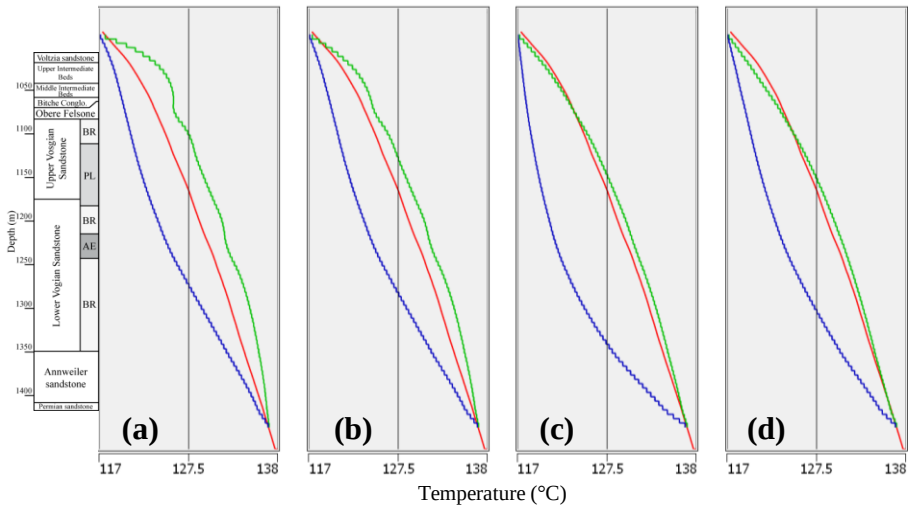

Figure 8: (a) temperature log at 10 m from the fault A, (b) temperature log at 20 m from the fault A, (c) temperature log at 40 m from the fault A, (d) temperature log at 80 m from the fault A; with measured temperature log in red, simulated temperature log for scenario 2 in blue and simulated temperature log for scenario 3 in green

5.4 Flow pattern

Looking at the distribution of flow rates through the simulation grid cells in steady-state flow conditions for scenarios 2 and 3 (Figure 9), the flow paths can easily be interpreted.

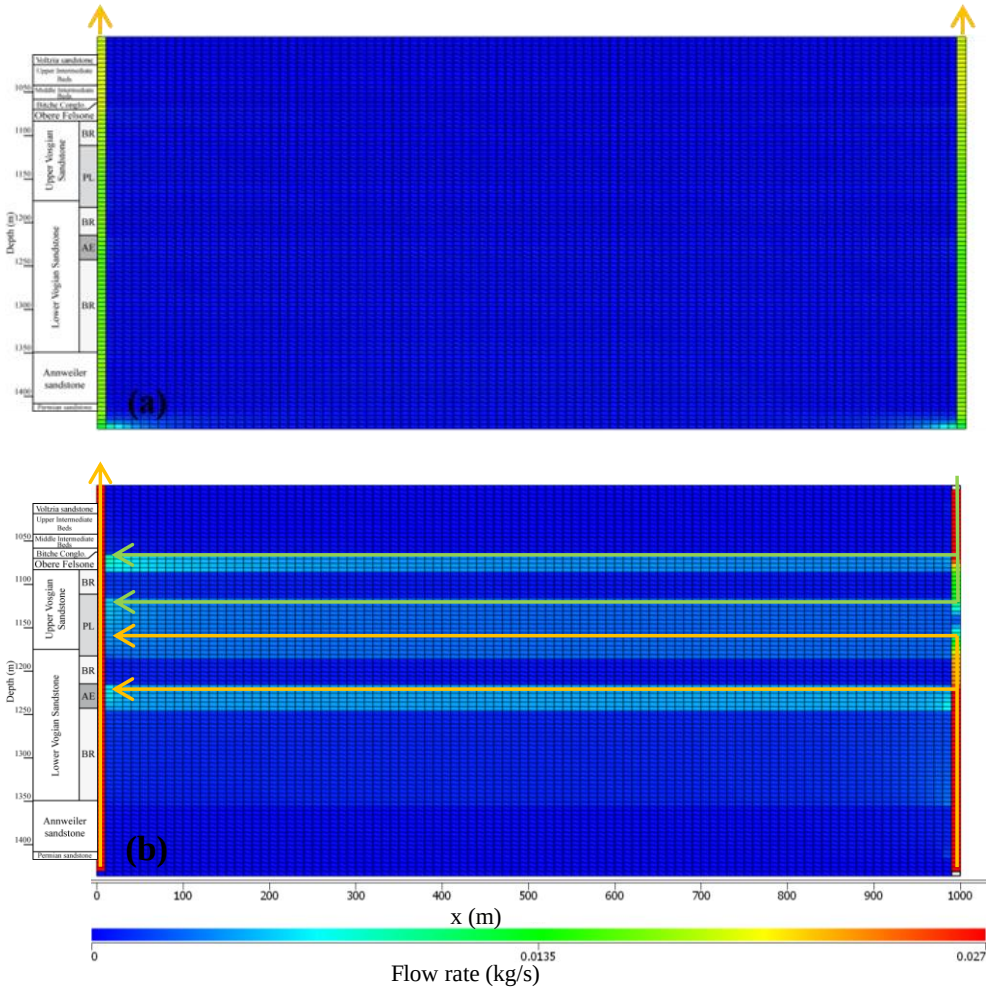

Figure 9: (a) Steady-state fluid flow rate through the cells for scenario 2 (non-connected conductive faults), (b) Steady-state fluid flow rate through the cells for scenario 3 (flow-connected conductive fault). The flow paths are indicated with arrows (orange for hot fluids coming from the bottom, green for warmer fluids coming from the top)

As expected, scenario 2 only generates flow through the two faults without any fluid exchange between the faults through the Buntsandstein formation, and scenario 3 gives rise to lateral flow through the three permeable sedimentary layers (Obere Felson as part of the Upper Buntsandstein, Playa Lake and fluvioaeolian). It can be noticed; however, that part of the fluids flowing through the sedimentary layers is likely to come from the overlying (necessarily warmer) aquifer(s) (Dezayes et al., 2007). Such an eventuality may be a concern to decide to produce geothermal fluids directly from the Buntsandstein formation.

5.5 Influence of prescribed pressure gradients

With no precise information available about the pressure (or hydraulic potential) distribution in the granite reservoir and in the overlying aquifer, which are flow-connected by the faults, the simulation of scenario 3 was repeated with different pressure boundary conditions as indicated in Table 2. For these new scenarios, the selected pressures at the top of the faults are the same as scenario 3. Only the bottom pressure conditions are changed. Though a more complete sensitivity analysis would have been required to better understand the various flow conditions, trend results can already be observed from these few additional simulations.

Table 2: Pressure and temperature boundary conditions applied to the top and the bottom of model for the additional scenarios

Scenario	Boundary condition	P (bar) Fault A	P (bar) Fault B	T (°C)
3.b	Top	96	101	117
	Bottom	136	146	137
3.c	Top	96	101	117
	Bottom	155	165	137
3.d	Top	96	101	117
	Bottom	155	175	137

Compared with scenario 3, scenario 3b involves smaller flow rates, whereas scenarios 3c and 3d correspond to higher and increasing flow rates. As seen in Figure 10, all the additional scenarios lead to temperature logs that further depart from the measured one. By decreasing the flow rates, too small temperatures are obtained, especially in the upper part of the model, whereas increased flow rates lead to excessive temperatures at all depths and all distances.

Among all simulated scenarios, scenario 3 best fits the measured temperatures and temperature gradient logs. Provided that the hydraulic properties assigned to the faults and to the permeable sedimentary layers are appropriate, the hydraulic gradient of 0.005 bar/m applied between the faults (5 bars over a distance of 1,000 m) can be interpreted as resulting from a structural dip of about 3°. Such a structural dip is consistent with that of about 5° measured in the Soultz-sous-Forêts area.

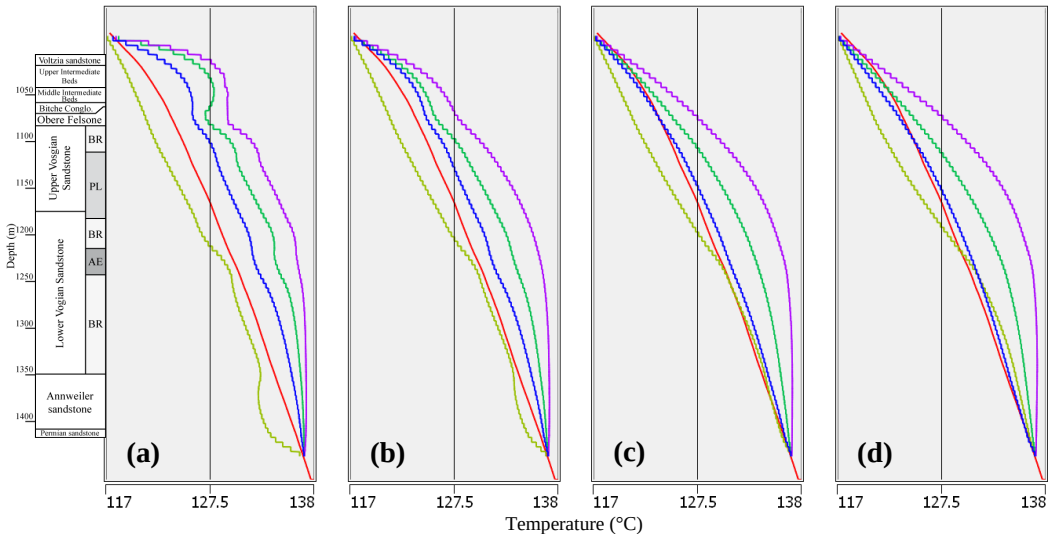

Figure 10: (a) Influence of the boundary conditions on the temperature log at a distance of 10m from fault A, (b) influence of the boundary conditions on the temperature log at a distance of 20m from fault A, (c) influence of the boundary conditions on the temperature log at a distance of 40m from fault A, (d) Influence of the boundary conditions on the temperature log at a distance of 80m from fault A; with measured temperature log in red, simulated temperature log for scenario 3 in blue, simulated temperature log for scenario 3.b in yellow, simulated temperature log for scenario 3.c in green, simulated temperature log for scenario 3.d in purple.

6. CONCLUSION

This study was an attempt to understand and explain temperatures and temperature gradient anomalies observed in the Buntsandstein formation along borehole EPS1. It confirms the presence of convective heat transport through the crossing faults reaching the underlying granite reservoir, but also through several permeable stratigraphic layers connecting the faults. The flow

boundary conditions of the numerical model that best fits the temperature data can be explained by a structural dip of about 3°, which is consistent with the measured dips in the Soultz-sous-Forêts area. From this study, information can also be derived about the distance of borehole EPS1 from the nearby fault and about the flow direction in the permeable layers with respect to this fault. The numerical models also show that water coming from the overlying aquifer(s) can be drained by upstream faults and reach the permeable sedimentary layers where it mixes with flowing geothermal water coming from the granite reservoir. Whether such a phenomenon is critical to production of geothermal fluid directly from the Buntsandstein formation is an aspect that would need to be confirmed. It could be studied as part of a 3D numerical reservoir model in order to assess the geothermal potential of the reservoir, depending on the number, locations and rates of producer and injector wells.

REFERENCES

Bächler, D., Khohl, T., and Rybach, L.: Impact of graben-parallel faults on hydrothermal convection - Rhine Graben case study, Physics and Chemistry of the Earth, 28, (2003), 431-441.

Bourquin, S., Guillocheau, F., and Peron, S.: Braided rivers within an arid alluvial plain (example from the Lower Triassic, western German Basin): recognition criteria and expression of stratigraphic cycles, Sedimentology, 56, (2009), 2235-2264.

Dezayes, C., Thinon, I., Courrioux, G., Tourlière, B., and Genter, A.: Estimation du potentiel géothermique des réservoirs clastiques du Trias dans le Fossé rhénan, Rapport Finale, BRGM/RP-55729-FR: 72p., (2007).

Edel, J.B., and Weber, K.: Cadomian terranes, wrench faulting and thrusting in the central Europe Variscides: geophysical and geological evidence, Geologische Rundschau, 84, (1995), 412-432.

Genter, A.: Géothermie roches chaudes sèches. Le granite de Soultz-sous-Forêts (Bas-Rhin, France). Fracturation naturelle, altération hydrothermales, et interactions eau-roche, Document du BRGM, n°185, Université d'Orléans, France: 201p., (1990)

Genter, A., Castaing, C., and Martin, P.: Assessment of reservoir fracturing from boreholes: comparison between core and wall-image data, Revue De l'Institut Francais Du Pétrole,52, (1997),45–60.

Genter, A., Guillou-Frottier, L., Breton, J.P., Denis, L., Dezayes, C., Egal, E., Feybesse, J.L., Goyeneche, O., Nicol, N., Quesnel, F., Quinquis, J.P., Roig, J.Y., and Schwartz, S.: Typologie des systèmes géothermiques HDR/HFR en Europe. Rapport final. BRGM/RP-53452-FR, 165 p., 75 fig., 10 tab., (2004).

Haffen, S.: Caractéristiques géothermiques du réservoir gréseux du Buntsandstein d'Alsace. Thesis University of Strasbourg, Strasbourg, France, 393p., (2012).

Haffen, S., Geraud, Y., Diraison, M. and Dezayes, C.: Fluid-flow zones in a geothermal sandstone reservoir: localization from thermal conductivity and temperature logs, borehole EPS1 (Soultz-sous-Forêts, France), Geothermics, 46, (2013), 32-41.

Kohl, T., Bächler, D. and Rybach, L.: Steps towards a comprehensive thermo-hydraulic analysis of the HDR test site Soultz-sous-Forêts, World Geothermal Congress, (2000).

Le Carlier, C, Royer, J.J., and Flores, E.L.: Convective heat transfer at the Soultz-sous-Forêts Geothermal Site: Implications for oil potential, First Break, 12, (1994), 553-560.

Munck, F., Walgenwitz, F., Maget, P., Sauer, K., and Tietze, R.: Synthèse géothermique du Fossé Rhénan Supérieur, Commission of the European Communities, BRGM Service Géologique Régionale d'Alsace - Geologisches Landesamt Baden-Württemberg, (1979).

Place, J., Diraison, M., Naville, C., Geraud, Y., Schaming, M., and Dezayes, C.: Decoupling of deformation in the Upper Rhine Graben sediments. Seismic reflection and diffraction on 3-component Vertical Seismic Profiling (Soultz-sous-Forets area), Comptes Rendus Geoscience, 342, (2010), 575-586.

Pribnow, D., Fesche, W., and Hägedorn, F.: Heat production and temperature to 5 km Depth at the HDR Site in Soultz-sous-Forêts, G.G.A. report: 17p., (1999).

Pribnow, D., and Schellschmidt, R.: Thermal tracking of upper crustal fluid flow in the Rhine Graben, Geophysical Research Letters, 27, (2000), 1957-1960.

Pruess, K., Oldenburg, C. and Moridis, G.: TOUGH2 User's Guide, Version 2.0., Lawrence Berkeley National Laboratory Report, LBNL-43134, (1999).

Schellschmidt, R., and Clauser, C.: The Thermal Regime of the Upper Rhine Graben and the Anomaly at Soultz, Zeitschrift für Angewandte Geologie, 42, (1996), 40-44.

Schumacher, M.E.: Upper Rhine Graben: Role of preexisting structures during rift evolution, Tectonics, 21, (2002), 17p.

Sizun, J.P.: Modification des structures de porosité de grès lors de transformations pétrographiques dans la diagenèse et l'hydrothermalisme. Thesis, Institut de Geologie. Strasbourg, Université Louis Pasteur, Strasbourg, France, 297 p., (1995).

Valley, B.: The relation between natural fracturing and stress heterogeneities in deep-seated crystalline rocks at Soultz-sous-Forêts (France), Thèse de l'Institut Fédéral Suisse de Technologie (ETH), Zurich, Suisse: 297p., (2007).

Vernoux, J.F., Genter, A., Razin, P., and Vinchon, C.: Geological and petrophysical parameters of a deep fractured sandstone formation as applied to geothermal exploitation, EPS-1 borehole, Soultz-sous-Forêts, France, BRGM Open file Report, R 38622: 69 p., (1995).

Vosteen, H.D., and Schellschmidt, R..: Influence of temperature on thermal conductivity, thermal capacity and thermal diffusivity for different types of rock, Physics and Chemistry of the Earth, 28, (2003), 499–509.